TRAPPED PARTICLE RESONANCE EFFECTS ON THE NTM DRIVEN LOSSES OF ENERGETIC PARTICLES

H. E. Ferrari,[1,2,*] R. Farengo,[1,3] P. M. Garcia-Martinez,[1,2,4] and C. Clauser[5]

[1] *Centro Atómico Bariloche (CAB), Comisión Nacional de Energía Atómica, Av. Bustillo 9500, 8400 Bariloche, Argentina.*
[2] *Consejo Nacional de Investigaciones Científicas y Técnicas (CONICET), Av. Bustillo 9500, 8400 Bariloche, Argentina.*
[3] *Universidad Nacional de Cuyo, Instituto Balseiro, Av. Bustillo 9500, 8400 Bariloche, Argentina.*
[4] *UNR, Sede Andina, Bariloche, Argentina.*
[5] *PPPL*

(Dated: April 9, 2021)

The $(2,1)$ neoclassical tearing mode (NTM) has been proposed as a candidate to explain the larger than expected losses of high energy ions produced by neutral beam injection observed in several experiments. Although the numerical simulations performed so far to study the effect of NTMs on energetic ions have reproduced several features observed in experiments, the agreement is not completely satisfactory. In particular, it has been difficult to reproduce the total amount of losses, which are affected by the details of the perturbation in the edge region. In this work we study the effect of NTMs on the confinement of energetic ions produced by NBI injection using the code FOCUS, a full orbit code that runs in Graphical Processing Units. This allows us to follow the evolution of a large number of particles with modest resources. A reconstruction technique that includes the experimental information available is employed to calculate the perturbed magnetic and electric fields. The main result of this study is that when the frequency of the NTM matches the toroidal precession frequency of the trapped particles ($f \sim E$), the losses increase significantly

PACS numbers: 52.55.Fa 52.55.Tn, 52.55.-s,
Keywords: Ion Losses; NTM

* ferrarih@cab.cnea.gov.ar

I. INTRODUCTION

Experimental and theoretical studies have shown that neoclassical tearing modes (NTM) can affect the confinement of fusion born alpha particles and high energy ions produced by NBI and ICRH [1–4]. Most numerical studies performed thus far involve following the trajectories of a large number of particles in the total electric and magnetic fields, sum of the equilibrium plus the perturbation produced by the NTM.

Carolipio et al. [1] studied the effect of NTMs on neutral beam current drive experiments in DIII-D. Significant reductions in the neutral beam current and neutron emission were observed when the modes were present. In the simulations, a birth population with a single energy was created and the Hamiltonian guiding center code ORBIT [5] used to follow beam ion trajectories in a numerical equilibrium with static magnetic islands. To model the tearing mode, a zero frequency, radially extended, single helicity perturbation was introduced in the simulations and allowed to act on the evolving birth distribution over time. The method employed to introduce the perturbation is the same as in Ref. [6]. In the simulations, the reduction in the neutral beam current drive and neutron emission were 35% and 40%, respectively. This is consistent with the measured reductions of $40 \pm 14\%$ and $40 \pm 10\%$. Several features of the lost particle distribution indicate that orbit stochasticity is the loss mechanism in the simulations and strongly suggest that the same mechanism is responsible for the losses observed in the experiment.

In [2], a beam code was used to calculate the initial positions and velocities of the ions and the ORBIT code to follow their trajectories. An axisymmetric equilibrium with circular cross section was employed and a $(2, 1)$ static magnetic perturbation was introduced, using the same form for the perturbed vector potential as in [1]. The simulation results reproduce the main experimental phenomenology and it was concluded that the overlapping of drift islands leads to orbit stochasticity and enhanced losses of passing fast ions.

Strumberger et al. [3] performed a complete numerical simulation of the same ASDEX discharge presented in [2]. A realistic 3D equilibrium that included toroidal field ripple was employed and the initial distribution of the high energy ions was simulated with a beam code. The magnetic field pertubation was introduced by an analytical ansatz but there was no electric field because a static perturbation was considered. Two $(2, 1)$ perturbations with different radial profiles were employed, and their amplitude adjusted to match the width of the experimentally observed magnetic islands. It was found that significant losses occurs only when the perturbation extends beyond the separatrix and that the lost particles are initially located very close to the last closed surface, far from the magnetic islands. A detailed analysis of the particle trajectories provided important information on the underlying loss mechanisms such as: (i) losses of passing particles caused by drift island formation, and (ii) losses of trapped particles due to stochastic diffusion.

Gobbin [4] performed a similar analysis with ORBIT but included the possibility of rotating islands. In this case, an electric potential was introduced to cancel the parallel component of the perturbed electric field, which is supposed to be shorted out by the electrons. A strong dependence of the losses on the radial profile of the perturbation was also found in this study. In particular, the shape of the perturbation and its derivative at the radius where the $(3, 1)$ resonance between the $(2, 1)$ NTM and the "drift orbit" occurs is critical. As in [3], all the particles lost in the simulations come from within 5 to 8 cm of the separatrix. The addition of island rotation does not seem to increase the number of lost particles but changes their toroidal distribution, which becomes uniform.

Kurki-Suonio et al. [7] studied the effect of NTMs and microturbulence on alpha particle confinement in ITER scenario 2 plasmas. They used a Hamiltonian formalism to derive the equation of motion in magnetic coordinates and introduced the magnetic islands by adding a perturbed vector potential parallel to the equilibrium magnetic field, as in [3]. Static (2,1) and (3,2) perturbations were considered, so there was no perturbed electric field. The orbit integration was carried out using a hybrid-method that combines guiding center (GC) following and full-orbit tracing. When an ion GC is found to be within a Larmor radius of the wall, the latest GC time step is cancelled and repeated by following the full Larmor orbit. Toroidal field ripple was not included in the NTM calculations because it can not be accommodated in the Hamiltonian formalism employed. Since the anomalous diffusion was not found to redistribute fast particles dramatically, the NTM simulations were carried out also without anomalous diffusion. Both NTMs were found to increase particle losses but the effect is strongest for the (2,1) mode. When both modes are included particle losses do no increase compared to the (2,1) only case, indicating that the modes are not coupled. Strong toroidal and poloidal variations in the particle flux across the separatrix (power load to the walls) were found.

All the studies reported above considered the interaction of the NTMs with the energetic ions but not the changes in the beam driven current, deposited torque and heat and the changes in the equilibrium that occur as a consequence of this interaction. A first attempt at including all these effects self-consistently was recently presented by Bardóczi et al. [8], who employed the TRANSP-Kick energetic particle transport code to study the effect of NTMs on DIII-D discharges with NBI. In the interpretation mode of TRANSP-Kick, the measured thermal profiles and the properties of the magnetic perturbations are given and the ORBIT code is employed to calculate the probability of changes in the energy and $\mathcal{P}$ of the energetic ions due to their interaction with the NTM. These probabilities are then used to modify the energetic ion distribution at every time step. The results show the existence of a strong dependence of

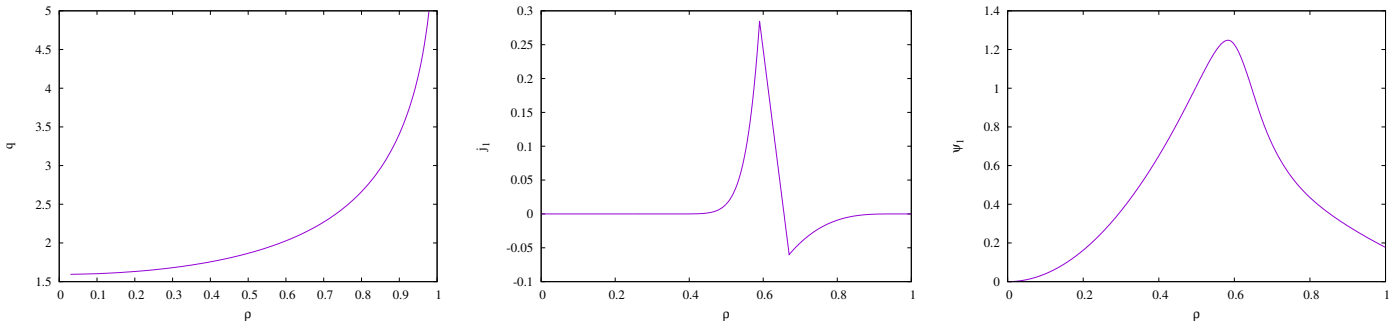

FIG. 1: Left: q profile, middle: pertubed current, right pertubed flux.

fast ion losses with the mode frequency, with a maximum between 30 and 40 kHz (see Fig. (9) in [8]), and a critical frequency for a core resonance to appear.

References [1–3] considered static perturbations, while a rotating mode with a fixed frequency was employed in [4]. In addition, except for the full orbit calculation used next to the wall in [7], all previous studies used guiding center codes. Since the high energy particles have large Larmor radius and orbit overlapping is considered to be responsible for the observed particle redistribution and losses, using the exact orbits can result in important changes.

Here we employ the full orbit code FOCUS [9] and study the effect of changing the mode frequency. In addition, the method employed to calculate the perturbed electric field is different from that used in [4] and [8]. We use Ohm's law, thus guaranteeing that, except for the resistive contribution, there are no components of the perturbed electric field parallel to the magnetic field. The main result of this study is that when the frequency of the NTM matches the precession frequency of the trapped particles ($f \sim E$), the losses increase significantly. According to our simulations, the main losses correspond to trapped particles (with average pitch at the loss point of 0.53). This is in accordance with experiments performed in ASDEX U [2], where the lost ions had a defined energy and pitch. The perturbed electric field changes the resonance frequency of trapped particles losses, and increase the maximun losses at resonance.

This paper is organized as follows, in section 2 we present the model of the NTM. In section 3, we present the results of a series of simulations for conditions which are similar to those of the experiments performed at ASDEX U. In section 4 we analyse our results and finally, in section 5 we summarize our results and discuss future research.

II. THE MODEL

The fields employed to calculate the trajectories are the sum of a 2D equilibrium magnetic field plus the 3D electric and magnetic fields produced by the NTM. The equilibrium magnetic field is obtained from the analytical magnetic flux derived by McCarthy to fit a series of ASDEX U discharges [10]. The major and minor radii are $R = 1.71$ m and $a = 0.51$ m respectively and the vacuum toroidal field at $r = R$ is $B_0 = 2.5$ T. The ion cyclotron frequency is used to normalize time and frequencies in the rest of this paper.. The perturbed magnetic flux produced by the NTM, Ψ_{pert}, is calculated employing the reconstruction technique proposed by Igochine [11]. In that paper, the perturbed current density J_{pert} is reconstructed using the experimental information available (i. e. width of the magnetic island, temperature profiles, etc), see equation (6) in [11]. Writing $J_{pert} = hJ_1(r)$, where h is a free parameter, Ψ_{pert} is then obtained by solving Ampere's law with the perturbed current density (J_{pert}). This calculation is performed in cylindrical coordinates. The q profile, J_{pert} and the calculated Ψ_{pert} are shown in figure 1, where $\rho = (1 - \Psi/\Psi_{max})$, Ψ is the equilibrium flux and Ψ_{max} is the flux at the last closed surface (LCS). A flux coordinate system, constructed with the method proposed by Jardin [6], is used to map the cylindrical perturbation to the equilibrium. We find that no spurious islands appear in the total magnetic flux provided that only one mode is included. In our case, the $(2, 1)$ dependence is taken to be $\exp(i2\theta + i\phi + \omega t)$, where θ is the poloidal angle, ϕ is the toroidal angle, ω is the normalized mode frequency and t is normalized time. We adjust the parameter h to match the island size. In figure 2 we show Poincare plots of the equilibrium (left) and perturbed (center) magnetic fields and a plot of the island size as a function of the parameter h. The perturbed case contains only the (2,1) mode. The perturbed electric field E_1 is calculated with the resistive Ohm's law, where the velocity is obtained from the displacement, which is parameterized as in eq. (2) of Ref. [11].

$$E_1 = -\frac{-\frac{\partial \xi}{\partial t} \times B_0}{c} + \eta J_{pert}, \tag{1}$$

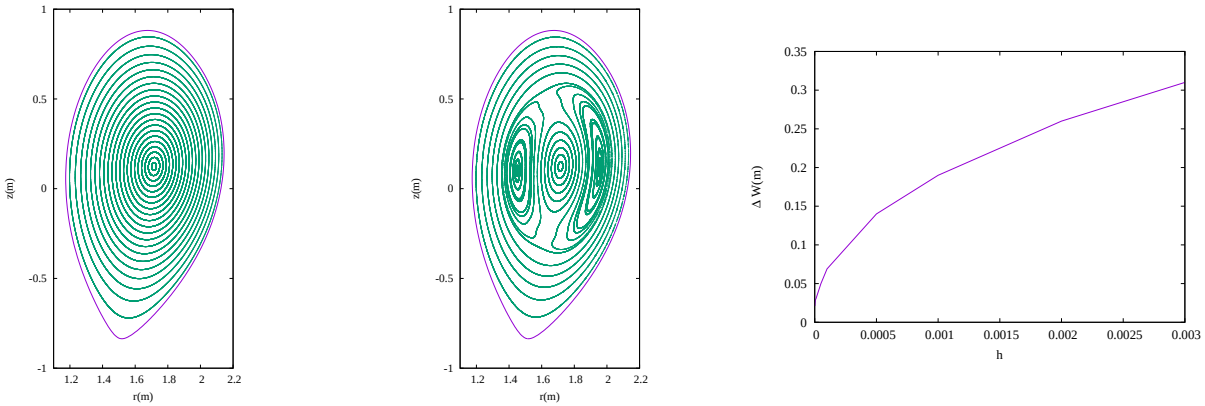

FIG. 2: Left: Poincare plot of the equilibrium magnetic field. Middle: Poincare plot of the equilibrium magnetic field plus perturbation. No spurious islands appear. Right: Island width as a funcion of the parameter h.

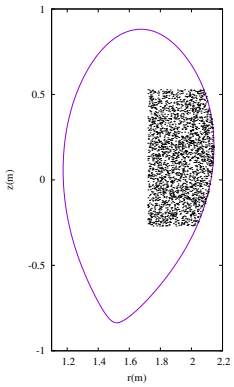

FIG. 3: Poloidal projection of the initial particle distribution. Each point indicates the initial position of a particle. The blue line is the LCFS. We plot one particle for every 100 particles.

where ξ is the displacement. The particles are considered as tracers and their trajectories are calculated by solving the full orbit equation with the total fields [9, 12].

In the experiment described in [2] the energetic ions were generated by Neutral Beam Injection (NBI). We emulate the initial NBI distribution with a collection of particles distributed as shown figure 3, with the same energy and pitch uniformly distributed between 0.2 and 0.9. In a typical run 250000 particles are evolved during 3.34 ms for each set of parameters using the code FOCUS that runs in GPUs [2]. When a particle reaches the last closed flux surface (LCFS) it is considered lost. When the energy is set to 70KeV and there is no perturbation 6.7% of the particles are early losses. 66.7% are passing particles and 26.6% are trapped particles. The passing and trapped particles are well confined.

III. RESULTS

Figure 4 shows the percentage of initially trapped and passing particles that are lost as a function of the normalized NTM frequency for two energies, 70 and 35 keV. The parameter h is fixed to $h = 0.001$, producing an island width of 19.3 cm (Figure 2 right). The toroidal precession frequency distribution of the trapped particles is also shown, with full boxes (70 keV in brown, 35 keV in cyan). The dependence of the toroidal precesion frequency (ω_t) with the energy can be appreciated in the figure ($\omega_t \sim E$). The losses of trapped ions peak when the toroidal precession frequency of the trapped particles is similar to the mode frequency. The passing particle losses, which are also shown in figure 4, are much smaller and have a very weak dependence on the mode frequency When the perturbation is reduced the losses are reduced as can be seen in figure 5.

Finally we collect the particles that are lost at a fixed toroidal position in figure 6. To produce this figure, we followed 330000 trapped particles. The frequency of the mode was set to the value that produces the maximum ion

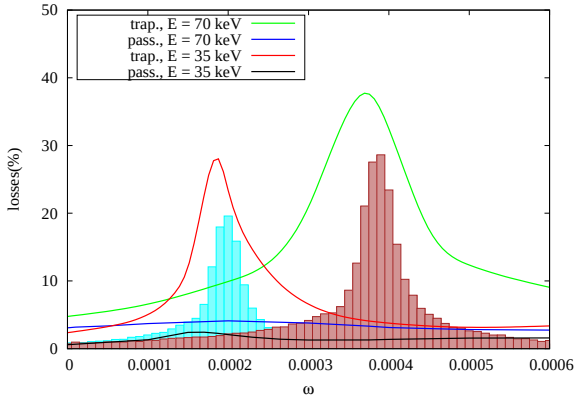

FIG. 4: Trapped and passing particles losses as a function of the normalized NTM frequency. The histograms shows the trapped toroidal precesion frequency. $h = 0.001$

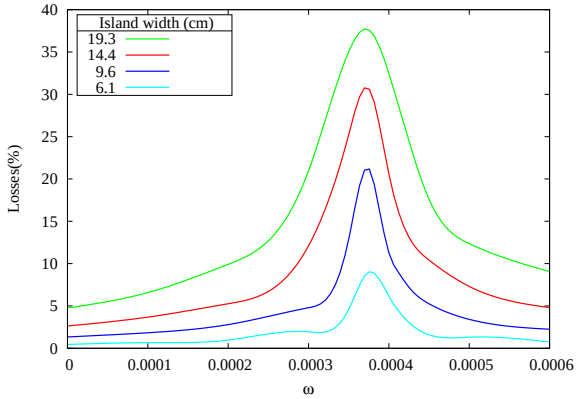

FIG. 5: Trapped ion losses for different island widths as a function of the normalized mode frequency. $E = 70$ keV.

losses ($\omega = 3.75 \times 10^{-4}$) and $h = 0.001$. We collect the particles that are lost with toroidal coordinate $[0, \pi/16]$. It is clear that the losses at a fixed position follow the NTM, the maxima have the same period as the NTM. The signal decreases because we do not replace the lost of particles.

Figure 7 shows the ions losses vs NTM frequency when both B_1 and E_1 are on. The maxima are displaced to higher frequencies as the amplitude of the electric field increases. The electric field of the NTM transfers energy to the particles increasing their average precession frequency. Figure 8 shows the histogram of ion losses vs energy and

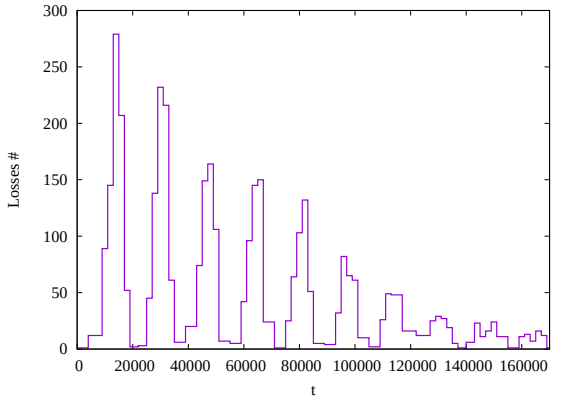

FIG. 6: Ion losses as a function of time at a fixed toroidal position. $E = 70$ keV.

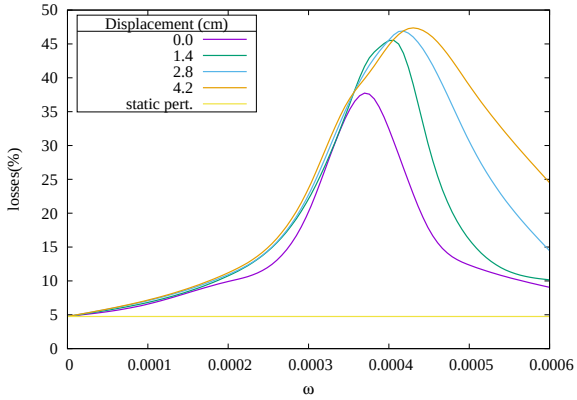

FIG. 7: Ion losses as a function of the NTM frequency when E_1 is on, for different displacement amplitudes.

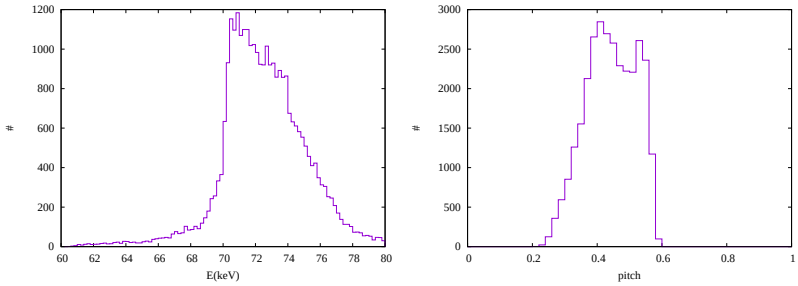

FIG. 8: histogram of ion losses vs energy (left) and vs pitch (right) at the time they are lost.

pitch of the particles at the time they are lost when B_1 and E_1 are on (E_1 with a displacement amplitude of 1.4 cm).

IV. IONS LOSSES MECHANISM

Figure 9, shows the poloidal projection of the trajectory of a trapped particle when B_1 is active for different NTM frequencies. When B1 is off, the bouncing point is fixed and the particle is well confined (fig. 9(a)). The bouncing point is highlighted with colored dots. The color indicates the time. When B_1 is on and static, the bouncing point oscilates but its average position remains basically the same as in the non perturbed case, as can be further aprreciated in fig 10(f). For other NTM frequencies the position of the bouncing point changes and its average position moves to higher z values. Finally, when the frequency of the mode matches the precession frequency ($\omega = 3.75 \times 10^{-4}$), the particle is lost (figure 9(e)). This is more clear when we plot the full orbit as in the right frame of the figure 9(f). The full orbit (in green) touches the LCS, but the GC orbit (in black) doesn't. In this case there is no electric field so the drift is due to the variation of the radial excursion following the magnetic lines caused by B_1 and an increase of the parallel velocity due to the modified mirror force [13].

Figures 10 (a)-(e) show the toroidal coordinate of the upper bouncing position for different NTM frequencies. The straigth line shows the phase of the NTM as a function of time in figures 10 (c)-(e), and the best fit in figures 10 (a)-(b) . Figure 10(a) shows the equilibrium case where, as expected, the toroidal precesion velocity is constant. When the pertubation is static 10(b) no changes are appreciated in the toroidal preccesion velocity. When the NTM rotates 10(c)-(e) the toroidal preccesion velocity changes, and in figure 10(e) a coupling between the toroidal preccesion velocity and the NTM can be appreciated. Finally in 10(f) we show the z coordiante of the upper bouncig position for different frequencies.

When the electric field is on the maximum of losses changes. The particles gain energy from the NTM, and consecuelntly the average toroidal precession frequency changes. The maxima also increase, this could be due to the $E_1 \times B$ drift.

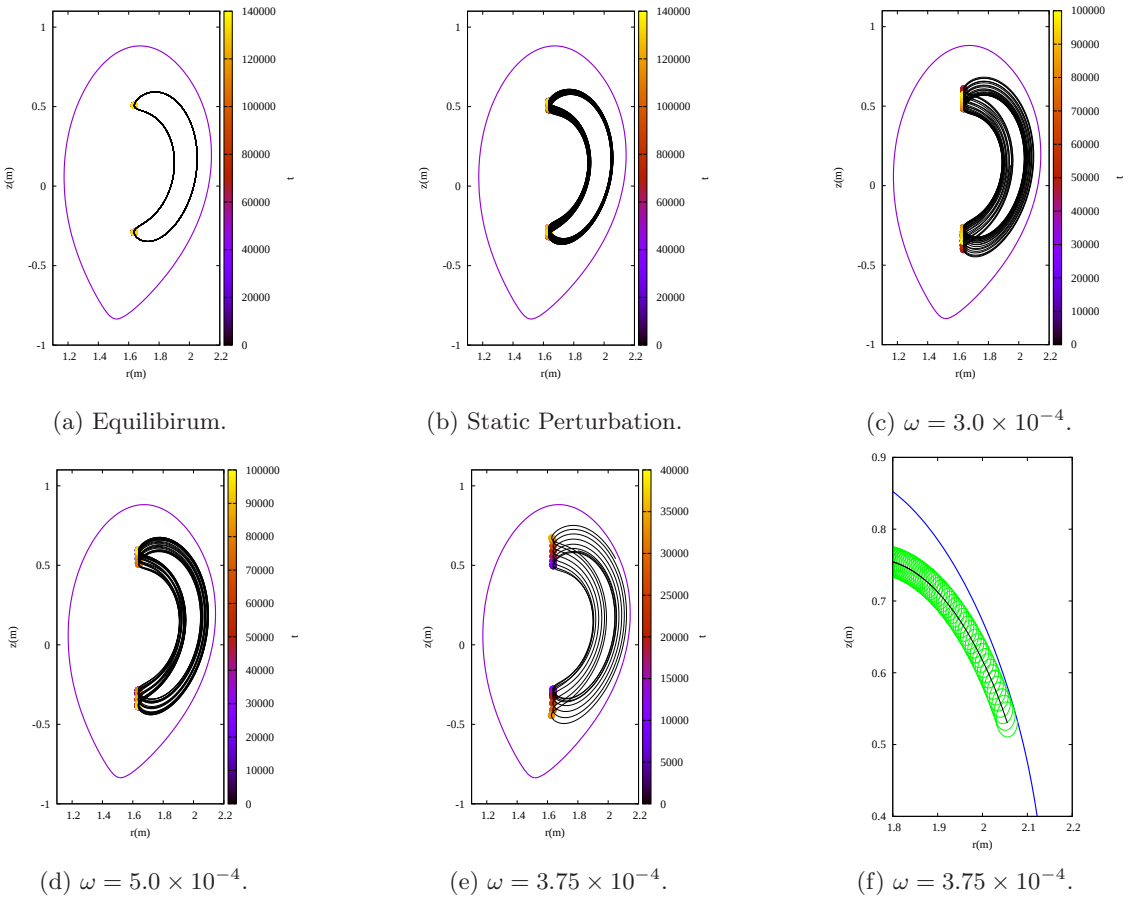

(a) Equilibirum. (b) Static Perturbation. (c) $\omega = 3.0 \times 10^{-4}$.

(d) $\omega = 5.0 \times 10^{-4}$. (e) $\omega = 3.75 \times 10^{-4}$. (f) $\omega = 3.75 \times 10^{-4}$.

FIG. 9: Orbit of a particle when B_1 is on for different NTM frequencies. When $\omega = 3.75 \times 10^{-4}$, frame (e), the particle is lost. The colored points indicate the bouncing position and the color scale is time. The LCFS is in blue and the full orbit in green. In (f), the full orbit (green line) touches the LCFS (blue line) but the GC orbit (black line) doesn't.

V. SUMMARY AND CONCLUSIONS

The main result of this study is that when the frequency of the NTM matches the precession frequency of the trapped particles, the losses increase significantly. According to our simulations, the main losses correspond to trapped particles (with average pitch at the loss point of 0.42). This is in agreement with experiments performed in ASDEX U [2], where the lost ions had a well defined energy and pitch. The losses of passing particles have a mild dependence of the mode frequency.

The perturbed electric field changes the resonance frequency of trapped particles losses, and increase the maximun losses at resonance. The effect of the eletric field is under investigation and will be discussed in a future paper.

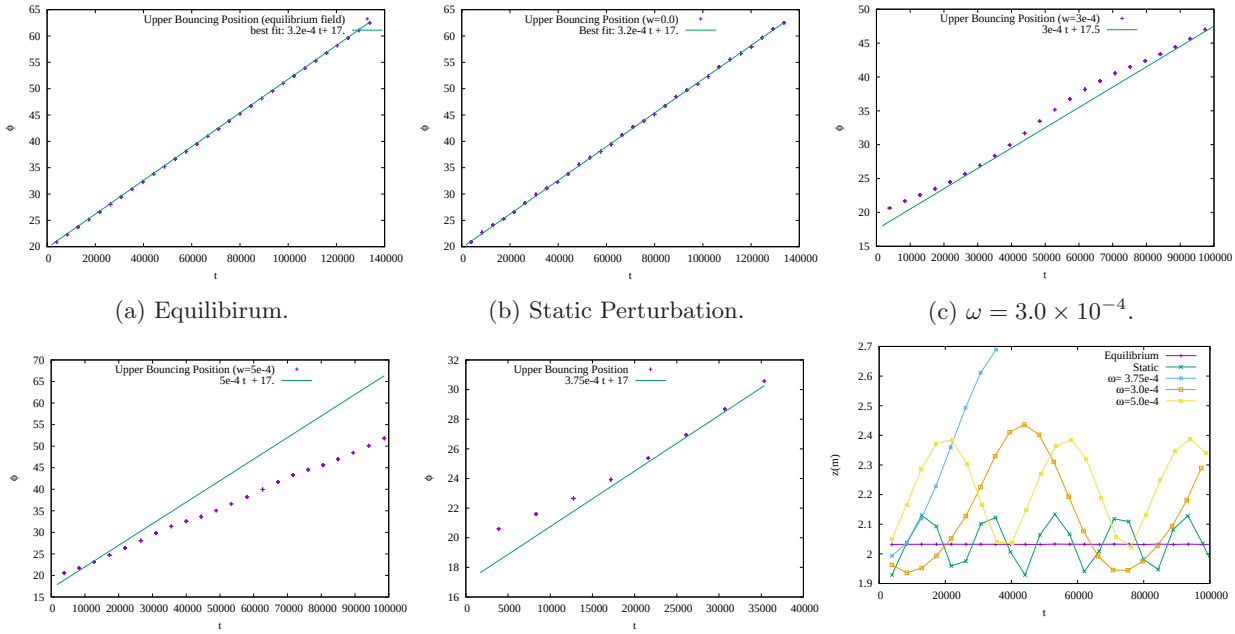

(a) Equilibirum. (b) Static Perturbation. (c) $\omega = 3.0 \times 10^{-4}$.

(d) $\omega = 5.0 \times 10^{-4}$. (e) $\omega = 3.75 \times 10^{-4}$. (f) z coordinate of the upper bouncing position

FIG. 10: (a)-(e) Toroidal coordinate of the upper bouncing position as function of time. The straight line is the phase velocity of the NTM in frames (c)-(e). (f) z coordinate of the upper bouncing position as a function of time.

[1] E. Carolipio, W. Heidbrink, C. Forest, and R. White, Nuclear Fusion **42**, 853 (2002).
[2] M. García-Muñoz, P. Martin, H.-U. Fahrbach, M. Gobbin, S. Günter, M. Maraschek, L. Marrelli, H. Zohm, and the ASDEX Upgrade Team, Nuclear Fusion **47**, L10 (2007).
[3] E. Strumberger, S. Günter, E. Schwarz, and C. T. and, New Journal of Physics **10**, 023017 (2008).
[4] M. Gobbin, L. Marrelli, H. Fahrbach, M. Garcia-Muñoz, S. Günter, P. Martin, and R. W. and, Nuclear Fusion **49**, 095021 (2009).
[5] R. B. White and M. S. Chance, The Physics of Fluids **27**, 2455 (1984), https://aip.scitation.org/doi/pdf/10.1063/1.864527.
[6] R. B. White, R. J. Goldston, K. McGuire, A. H. Boozer, D. A. Monticello, and W. Park, The Physics of Fluids **26**, 2958 (1983), https://aip.scitation.org/doi/pdf/10.1063/1.864060.
[7] T. Kurki-Suonio, O. Asunta, E. Hirvijoki, T. Koskela, A. Snicker, T. Hauff, F. Jenko, E. Poli, and S. Sipilä, Nuclear Fusion **51**, 083041 (2011).
[8] L. Bardóczi, M. Podestà, W. W. Heidbrink, and M. A. V. Zeeland, Plasma Physics and Controlled Fusion **61**, 055012 (2019).
[9] C. Clauser, R. Farengo, and H. Ferrari, Computer Physics Communications **234**, 126 (2019).
[10] P. J. Mc Carthy, Physics of Plasmas **6**, 3554 (1999), https://doi.org/10.1063/1.873630.
[11] V. Igochine, S. Günter, M. Maraschek, and the ASDEX Upgrade Team, Nuclear Fusion **43**, 1801 (2003).
[12] R. Farengo, H. Ferrari, M.-C. Firpo, P. Garcia-Martinez, and A. Lifschitz, Plasma Physics and Controlled Fusion **54** (2012), 10.1088/0741-3335/54/2/025007.
[13] E. Poli, M. García-Muñoz, H.-U. Fahrbach, and S. Günter, Physics of Plasmas **15**, 032501 (2008), https://doi.org/10.1063/1.2890771.